Programmable Dynamic Shapes with a Swarm of Light-Powered Colloidal Motors

Meiling Chen, Zhihua Lin, Mingjun Xuan, Xiankun Lin, Mingcheng Yang,* Luru Dai* and Qiang He*

Abstract: *We report robust control over the dynamic assembly, disassembly, and reconfiguration of light-activated molybdenum disulfide (MoS_2) colloidal motor swarms with features not possible in equilibrium systems. A photochemical reaction produces chemical gradients across the MoS_2 colloidal motors to drive them to move. Under illumination of a gradient light, these colloidal motors display a positive phototactic motion. Mesoscale simulations prove that the self-diffusiophoresis induced by the locally consumed oxygen gradient across MoS_2 colloidal motors dominates the phototactic process. By programming the structured illumination, the collective migration and well-defined shapes of colloidal motor swarms can be externally regulated. The successful realization of programmable swarm transformation of colloidal motors like the emergent behaviors of living systems in nature provides a direct proof-of-concept for active soft materials and systems, with adaptive and interactive functions.*

Introduction

In nature, individual living organisms interact locally with neighbours and self-organize into various complex dynamic patterns without centralized control by leaders, exhibiting fascinating features such as cohesion, robustness, flexibility and collective intelligence.[1–3] Typical examples include flocks of birds,[4,5] schools of fish,[6] swarms of locusts,[7] troops of fire ants,[8] bacterial colonies,[9] and other active systems.[10] These collective behaviours allow them to better adopt the surrounding environments or accomplish complex tasks that could not be achieved by individuals. In these bio-systems of collective navigation, there is a phase transition from disordered to ordered states as the density increases.[7] Inspired by these emergent properties in biology, artificial colloidal motors are increasingly being considered due to their good controllability, synthetic diversity and ability to autonomously propel themselves, and their collective self-organization into dynamic structures and swarms in a non-equilibrium manner.[11–14] They are thought as ideal candidates for applications in the fields of active target delivery, smart devices and living printing.[15,16] Recent efforts in studying the collective behaviour of out-of-equilibrium systems include systems driven by externally physical fields (electric, magnetic or light) and internally chemical triggers.[17–21] Particularly, light offers a method for controlling swarms in both space and time. Recently, light-driven collective motion has received more interests since swarms can be instantaneously triggered, and turned off remotely.[22–27] Studies focusing on light-activated swarms mainly involve photoacid generators, hematite, metals, AgCl, Ag_3PO_4, and Janus materials.[28–30] In these systems, diffusiophoresis of the colloidal motors and osmotic flows along the substrate are generated by the chemical imbalance, and driving the motion of colloidal motors towards or away from light.[28,31] Although the self-assembly of colloidal motors into clusters has already been demonstrated,[32] reconfigurable swarms of colloidal motors which mimic collaboration of living organisms and can be programmed to arrange into dynamic shapes still remain a challenge.

Herein, we demonstrate programmable self-organization of complex structures with MoS_2 colloidal motor swarms under UV light exposure. The MoS_2 colloidal motors autonomously move due to the self-diffusiophoresis and

---

[*] Dr. M. Chen, Dr. Z. Lin, Dr. M. Xuan, Dr. X. Lin, Prof. Q. He
Key Lab of Microsystems and Microstructures Manufacturing,
Harbin Institute of Technology
XiDaZi Street 92, Harbin 150001 (China)
E-Mail: qianghe@hit.edu.cn

Prof. M. Yang
Beijing National Laboratory for Condensed Matter Physics and
Laboratory of Soft Matter Physics, Institute of Physics, Chinese
Academy of Sciences
Beijing 100190 (China)
and
School of Physical Sciences, University of Chinese Academy of
Sciences
Beijing 100049 (China)
and
Songshan Lake Materials Laboratory
Dongguan, Guangdong 523808 (China)
E-Mail: mcyang@iphy.ac.cn

Prof. L. Dai
CAS Key Laboratory for Biomedical Effects of Nanomaterials and
Nanosafety and CAS Center for Excellence in Nanoscience, National
Center for Nanoscience and Technology
Beijing 100190 (China)
and
Zhejiang Engineering Research Center for Tissue Repair Materials,
Wenzhou Institute, University of Chinese Academy of Sciences
Wenzhou 325000 (China)
and
Oujiang Laboratory
Wenzhou 325000 (China)
E-Mail: dai@nanoctr.cn

Supporting information and the ORCID identification number(s) for
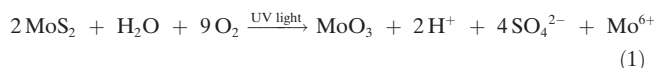the author(s) of this article can be found under:
https://doi.org/10.1002/anie.202105746.

osmotic flow induced by the substrate, which are generated by photochemical reaction. The collective motion of MoS_2 colloidal motors on negatively charged and positively charged surfaces further verifies that the diffusiophoresis induced by the O_2 gradient dominates the positive phototaxis of colloidal motors, which is consistent with the mesoscale simulation. Individual MoS_2 colloidal motors collectively create controllable and reversible assembly or disassembly. Living patterns of MoS_2 colloidal motors with sharp features and complex structures were programmed using a homemade structured illumination system. The collective intelligence of colloidal motors achieved shape transformation, which provides a versatile strategy for possible applications of intelligent micromachines and soft materials.

Results and Discussion

MoS_2 colloidal motors were synthesized using a facile solvothermal reaction of ammonium tetrathiomolybdate $((NH_4)_2MoS_4)$ according to a previously reported method.[33] Subsequently, MoS_2 colloidal motors with uniform diameters were obtained using a gradient centrifugation. The scanning electron microscopy (SEM) image in Figure 1 A shows that the diameter of the as-synthesized MoS_2 colloidal motors is ca. 257 nm with dimensional homogeneity. The inset image in Figure 1 A shows a typical transmission electron microscopy (TEM) image of a MoS_2 colloidal motor with folded edges and spherical morphology. The particle size distribution measured with a dynamic light scattering instrument (Figure 1 B) further shows that the resulting MoS_2 colloidal motors exhibit monodispersity (0.057) and a uniform size with an average diameter of 260 ± 21 nm. Figure 1 C (black curve) shows the zeta potential of the MoS_2 colloidal motors went up with the illumination time of UV light (340–380 nm). The initial zeta potential in water was measured as -77 mV, whereas increased to -38 mV after 12 min exposure. Accord-

ingly, the pH value of MoS_2 colloidal motor suspensions decreased from 7.45 to 6.68 with the increasing illumination time (blue curve), indicating the appearance of some kinds of photochemical reactions on the surface of MoS_2 colloidal motors. Furthermore, inductively coupled plasma mass spectrometry (ICP-MS) were conducted to examine the change of Mo and S in solutions before and after UV light exposure. As shown in Table S1, after 30 min irradiation, the amounts of S and Mo in solutions significantly increased from 4.036 to 49.50 mg L^{-1} and from 1.096 to 59.76 mg L^{-1}, respectively, confirming the decomposition of MoS_2 colloidal motors upon UV exposure. In addition, Figure 1 D shows that the density of dissolved oxygen in the MoS_2 colloidal motor suspension obviously decreased with light illumination (pink), whereas the pure water under UV light illumination exhibits negligible change. It is supposed that the photochemical reaction of MoS_2 colloidal motors in water is an oxygen-consuming process.

To further verify the reaction mechanism, X-ray photoemission spectroscopy (XPS) was employed to determine the chemical state of MoS_2 colloidal motors before and after UV light irradiation (45.8 mW cm^{-2}) for 10 min. As shown in Figure 1 E, F, for the pristine sample, the strong Mo3d A, S2s and S2p A at 227.2, 224.5 and 161.5 eV, respectively, indicate the dominant existence of Mo^{4+} and S^{2-} features in normal MoS_2. However, the presence of the Mo3d B band (231.2 and 233.8 eV) assigned to Mo^{6+} and the S2p B band (166.2 and 169.3 eV) assigned to S^{6+} indicates that small amounts of oxide species also exist in the pristine MoS_2 colloidal motors.[33] After light irradiation, some of the S^{2-} and Mo^{4+} were converted to the higher oxidation states of S^{6+} and Mo^{6+}, respectively (Table S2 and S3). Taken together, the increase of the zeta potential is assumed to be caused by the adsorption of Mo^{6+} on the surface of MoS_2 colloidal motors. Upon the illumination of UV light, the MoS_2 colloidal motors are assumed to be prone to be oxidized by oxygen, accompanying decompose of water. Parts of sulfur on the MoS_2 colloidal motors were released from the surface into solution, and the oxidized sulfur combined with the oxygen to form sulfate ion and MoO_3. The MoS_2 on the surface of colloidal motors is oxidized into MoO_3 with Mo^{6+} adsorbed on the surface, and H^+ is released into the solution. Therefore, the possible redox reaction may be given in Equation (1) as follows,

$$2\,MoS_2 \;+\; H_2O \;+\; 9\,O_2 \;\xrightarrow{\text{UV light}}\; MoO_3 \;+\; 2\,H^+ \;+\; 4\,SO_4^{2-} \;+\; Mo^{6+} \tag{1}$$

An Olympus optical microscope with a built-in illumination source was used to monitor the kinematic behaviour of MoS_2 colloidal motors at an extremely low surface density ($\varphi = 0.34\,\%$). The mean square displacement (MSD) of MoS_2 colloidal motors versus time intervals under exposure to UV light (red curve) is significantly greater than that without UV light irradiation (black curve) as shown in Figure S1. According to the above chemical reaction Equation (1), under illumination of UV light, a photocorrosion reaction on the surface of MoS_2 colloidal motors occurs, which consumes O_2 and generates MoO_3, H^+, SO_4^{2-} and Mo^{6+}. Given that the
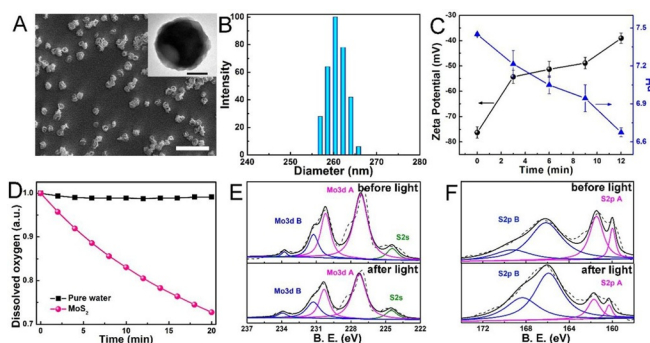

Figure 1. Experimental characterization of light-activated MoS_2 colloidal motors. A) SEM image of MoS_2 colloidal motors. Scale bar, 1 μm. The inset in (A) is a TEM image of a MoS_2 colloidal motor. Scale bar, 100 nm. B) Dynamic light scattering of MoS_2 colloidal motors. C) Variation of zeta potential (black) and pH (blue) in the MoS_2 colloidal motor suspension plotted as a functions of UV light irradiation time. D) Dissolved oxygen versus the irradiation time of pure water (black) and MoS_2 colloidal motor suspension (pink). E, F) XPS spectra of MoS_2 colloidal motors before (upper rows) and after (bottom rows) exposure to UV light (45.8 mW cm^{-2}) for 10 min.

structure of MoS$_2$ colloidal motors is not completely symmetrical, the photocorrosion reaction around the colloidal motors should be imbalanced. As a result, the imbalanced reaction across the MoS$_2$ colloidal motors provides the self-propelling force like previous reports.[28,31] We further explored the phototactic behaviour of light-powered MoS$_2$ colloidal motors by use of the optical microscope under exposure of UV light gradient. The time-lapse images in Figure 2 A, taken from Video S1, show the continuous motion of MoS$_2$ colloidal motors toward the central position of UV light on a negatively charged substrate, suggesting a positively phototactic motion. Similarly, MoS$_2$ colloidal motors also exhibit a positively phototactic motion on the positively charged substrate (by coating 3-aminopropyltrimethylsilane) as illustrated in Figure 2 B. Note that, at the initial time of light irradiation, a depletion region first occurred within the irradiation area, and then a circular MoS$_2$ pattern formed with a lower density than that of the pattern produced on a negatively charged substrate.

To obtain more information, particle image velocimetry (PIV)[9] was used to analyse the motion of MoS$_2$ colloidal motors in successive image frames. The raw images of MoS$_2$ colloidal motors were overlaid with velocity vectors, which show an axis-symmetric flow field (Figure S2 and Video S2). The calculated radial velocity as a function of radial position in Figure 2 C indicate that the MoS$_2$ colloidal motors beyond the light-exposed region (ca. 160–350 μm from the centre of the light spot) moved towards the light spot with a stable speed (ca. 6–7 μm s^{-1}). When colloidal motors aggregated and

formed patterns with a dynamic steady state, however, the average velocity of the colloidal motors in the centre of the pattern approached zero. This phenomenon is probably due to the reactant (dissolved oxygen) in the pattern being exhausted quickly, leading to the chemical reaction stopping. Meanwhile, MoS$_2$ colloidal motors are caged by inter-particle excluded volume and electrostatic repulsive interactions. MoS$_2$ colloidal motors show different variations in the colloidal motor density in the presence of the same UV light on two different charged substrates. The colloidal motor density (C) was normalized by initial density of colloidal motors (C_0) in the absence of UV irradiation. On the negatively charged substrate, Figure 2 D shows that the C/C_0 of the aggregate of MoS$_2$ colloidal motors increases with irradiation time, and the circular MoS$_2$ pattern was formed with a maximum C/C_0 of ca. 5.5 after 5 min of irradiation. However, on the positively charged substrate, the C/C_0 in the illumination region first decreases and then increases during assembly processing (Figure 2 E). After exposure for 5 min, the maximum C/C_0 reached ca. 2.5, which is much lower than that of the negatively charged substrate. Subsequently, on the positively charged substrate, the motor density in the close-up region away from the centre of light of ca. 100 μm^2 (Figure 2 F) decreases to ca. 0.27 in the initial stage (irradiation time less than 1 min) and then increases slowly. In contrast, the motor density increases monotonically on the negatively charged substrate.

The positively phototactic behaviour should be originated from the gradually increasing intensity of photochemical reaction along the UV light gradient. As schematically illustrated in Figure S3, the photochemical reaction on the MoS$_2$ colloidal motors which consumes a mass of O$_2$ and generates MoO$_3$, H$^+$, SO$_4^{2-}$ and Mo^{6+}, gradually increased along the gradient distribution of UV light. These chemical gradients induce three effects: electrophoretic, electroosmotic and diffusiophoretic effects, which competitively dominate the collective motion of MoS$_2$ colloidal motors to the irradiated region.[34,35] From the electrophoretic and electro-osmotic point of view, the diffusion rate of H$^+$ ($D = 9.31 \times 10^{-5}$ cm^2 s^{-1}) is greater than that of Mo^{6+} ($D = 0.51 \times 10^{-5}$ cm^2 s^{-1}) and SO$_4^{2-}$ ($D = 0.955 \times 10^{-5}$ cm^2 s^{-1}),[34] which induces a net electric field (E) pointed inwards (blue arrow). The electric field results in outwards electrophoresis of negatively charged MoS$_2$ colloidal motors. However, since the magnitude of the glass slide zeta potential (−85 mV) is greater than that of MoS$_2$ colloidal motors, the osmotic flow can overcome electrophoretic motion and has a significant role in driving MoS$_2$ colloidal motors towards the light spot. Regarding the diffusiophoretic effect of non-electrolytic O$_2$ molecules ($D = 1.97 \times 10^{-5}$ cm^2 s^{-1}), the concentration gradient of O$_2$ caused by the consumption of O$_2$ induces an imbalance osmotic pressure that propels the MoS$_2$ colloidal motors inwards. In fact, when the focal plane of the microscope was tuned so that the osmotic effect generated by the substrate was negligible, the MoS$_2$ colloidal motors in the bulk still actively accumulated in the illumination region (Figure S4 and Video S3).

To verify the mechanism, particle-based mesoscale simulations that properly involve the diffusiophoresis and osmotic
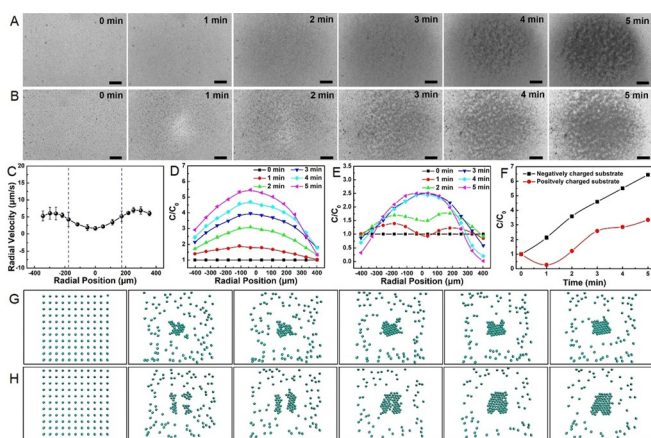

Figure 2. Collective behaviour and mechanism of light-powered MoS$_2$ colloidal motors. Time-lapse optical microscopy images of pattern formed on a negatively charged substrate (A) and a positively charged substrate (B). Scale bars, 100 μm. Rounded MoS$_2$ pattern created on negatively or positively charged substrates using a UV light source (intensity of ca. 7 mW cm^{-2}) with a circular light spot. C) The radial velocities corresponding to the radial position, in which the blue lines show the sites of the pattern boundary. Evolutions of colloidal motor density (C/C_0) versus radial position on the negatively charged (D) and positively charged substrate (E). F) A close-up count of the density with time extension at the centre of the pattern with a measured area of 100 μm^2. Numerical simulations of positively phototactic motion on on a negatively charged substrate (G) and a positively charged substrate (H). The number of colloidal motors in the simulations is 120.

flow were carried out. In the initial stage of light illumination, the electroosmotic flow rapidly dominates the aggregation (negatively charged substrate, Figure 2G and Video S4) or exclusion (positively charged substrate, Figure 2H and Video S5). It means that the electroosmotic flow generated by the positively charged substrate is directed outwards from the irradiation centre, which is the opposite direction for the case of the negatively charged substrate. However, as the exposure time increases (ca. 60 s), a shielding effect on the substrate charge is generated due to the increasing concentration of ions produced from the photocorrosion reaction. As a result, the functioning of the electroosmotic flow weakens, and the diffusiophoresis has a significant role that drives the gathering motion of the colloidal motors. These simulations are completely consistent with our experimental observations. Taken together, both the diffusiophoretic and electroosmotic effect contribute the positively phototactic motion of MoS_2 colloidal motors, whereas the oxygen concentration gradient-induced self-diffusiophoresis is dominant.

To verify the above-proposed phototacitc mechanism, a rectangularly gradiented UV light resource was empolyed. Time-lapsed images in Figure 3A show that MoS_2 colloidal motors collectively migrate towards the light and gradually form a rectangular-shaped MoS_2 motor swarm. As time passes, the colour of the rectangular motor swarm darkens, implying that more MoS_2 colloidal motors accumulated in the structured light spot region (Figure 3A). As demonstrated in Figure 3B and Video S6, a simulation was performed to reproduce the evolution of the MoS_2 motor swarm. The colloidal motor density (C/C_0) at peripheral regions of the pattern is plotted as a function of distance from the boundary (Figure 3C), which shows that density increases with distance. The SEM images of the obtained MoS_2 pattern in Figure 3D and E show that MoS_2 colloidal motors assembled together
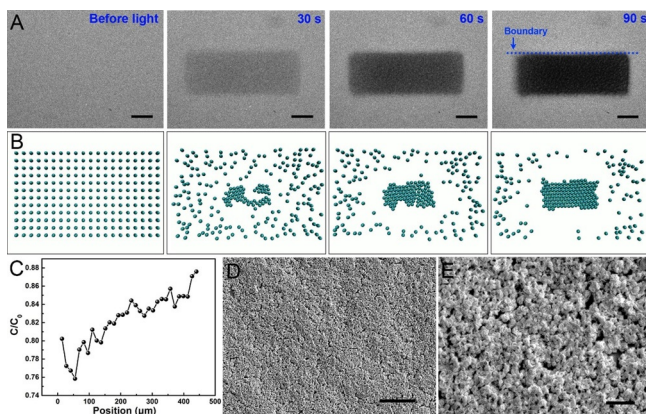
and formed a compacted MoS_2 layer, and the density of MoS_2 monolayer in the centre (Figure 3E) was much higher than that in the boundary zone (Figure S5). Both the experimental observations and the simulation eliminated the thermophoretic mechanism.

Finally, a homemade structured illumination system (Figure S6) was employed to generate a programmable transformation of MoS_2 colloidal motor swarms like the emergent behaviours of living systems. As shown in Figure 4A, MoS_2 colloidal motors on a negatively charged substrate were exposed to a structured light, which can actively drive them to assemble into a swarm with a desired shape. Time-lapsed images in Figures 4B–D show a well-defined MoS_2 swarm with „runner" shape appeared clearly. The dynamic self-organization process of „runner"-shaped MoS_2 colloidal motor swarms was reversible, in which „runners" could automatically vanish within 60 s after switching off the light due to Brownian motion (Figure 4E). Such „runners" can be rebuilt by projecting light again (Figure 4F, G). Following a 60 s absence of light, the „runner"-shaped MoS_2 motor swarm dispersed again (Figure 4H). This procedure could be repeated over many cycles as presented in Video S7. Furthermore, Figure 5 demonstrates that a transformation behaviour like the running process of the „runner" could be reproduced by altering the structured illumination. Light spots with desired input structures were sequentially projected onto the colloidal motor suspension, forming reversibly switched postures within 60 s. First, a standing „runner" emerged within 60 s driven by an illumination with the standing structure (Figure 5B). When light was then switched to running posture at 61 s, colloidal motors responded immediately, and the living „runner" transformed its posture from standing to running (Figure 5B–D). Upon switching to next structured illumination, the „runner" swung its arms and legs in another running posture (Figure 5E, F). The „runner"
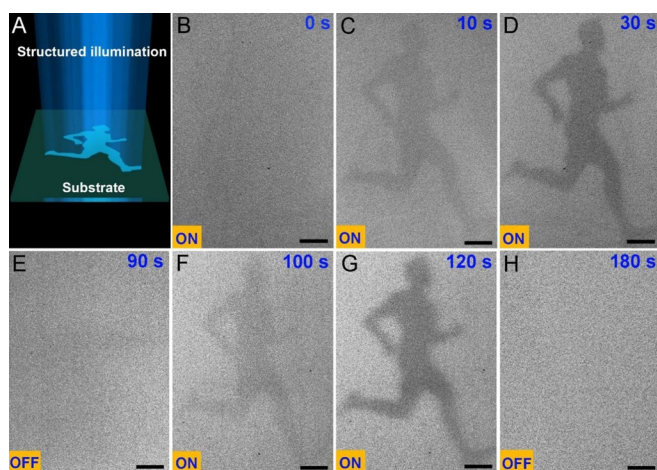

Figure 3. Rectangular patterning with MoS_2 colloidal motors. A) Forming process of rectangular swarms of MoS_2 colloidal motors upon exposure of rectangularly gradiented UV light resource, and B) corresponding numerical simulation. The light intensity is ca. 20 mWcm^{-2}. The blue line in (A) indicates the site of the pattern boundary. All scale bars, 200 μm. C) Density gradient analysis of MoS_2 colloidal motors for peripheral areas of the rectangular MoS_2 pattern that is light exposed for 90 s. On the *x*-axis, 0 μm is defined as the pattern boundary, and positions > 0 μm are regions further from the boundary. D, E) SEM images of MoS_2 aggregation in the inner area of the pattern. Scale bars are 5 μm and 1 μm, respectively.

Figure 4. Dynamic assembly of „runners" with MoS_2 colloidal motors. A) Schematic illustration of „runner"-shaped MoS_2 colloidal motor swarms using a structured UV light. B–D) The MoS_2 colloidal motors collectively exhibited a „runner" shape and E) disassembled rapidly when the light was switched off. F, G) The „runner" was recreated when the light was applied again. H) When the light was turned off, the colloidal motors diffused within 60 s. The light intensity is ca. 20 mWcm^{-2}. Scale bars, 200 μm.
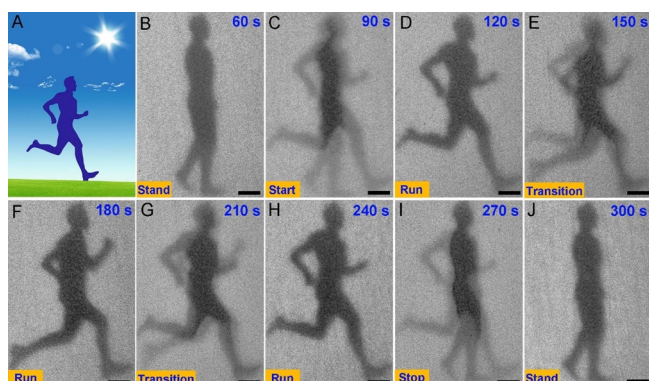
Figure 5. Transformation process of the „runner". A) Scheme illustrating that the living self-organization of active MoS_2 colloidal motors can realize the running process of a living hominoid „runner". B–D) By transforming the structured illuminations, the living „runner" transformed from a standing to a running posture, and E, F) swinging of arms and legs in another running posture. G–J) Following transformation of serial postures, the „runner" finally presented a standing posture. The light intensity is ca. 20 mWcm^{-2}. Scale bars, 200 μm.

finally presented a standing posture following transformation of serial postures (Figure 5 G–J). This dynamic transformation process of MoS_2 colloidal motor swarms was presented in Video S8.

Conclusion

We have demonstrated the collectively reconfigurable behaviour of light-activated MoS_2 colloidal motors with adaptive and interactive functions. The MoS_2 colloidal motors in the presence of dissolved oxygen and UV light could autonomously swim and also show the positively phototactic motion since the chemical reactions across MoS_2 motors occurred. This photocorrosion on the surface of MoS_2 motors generated multiple chemical gradients that caused the self-electrophoresis, self-diffusiophoresis and osmotic flow along the substrate. Further experimental results and numerical simulations verify that both the self-electrophoresis and osmotic flow may be neglected in this system, whereas the propelling force of the phototactic motion was mainly contributed by the oxygen gradient-induced self-diffusiophoresis. The phototactic MoS_2 colloidal motors could collectively self-organize to form well-defined dynamic „rectangle" or „runner" structures under programmable modulation of the structured UV light resource. The dynamic assembly and disassembly of these structured motor swarms could be repeated over many cycles and the dynamic transformations of serial „runner" postures could be achieved conveniently by projecting the structured illumination. Therefore, the MoS_2 colloidal motors can collectively self-organize into two dimensional and visual swarm structures like the emergent behaviors of living systems, which provides a state-of-the-art solution to prepare reconfigurable colloidal motor swarms with well-defined dynamic structures and locomotion and thus hold a potential in the fields of next-generation intelligent materials and micro/nanotechnology.

Conflict of interest

The authors declare no conflict of interest.

[1] J. Halloy, G. Sempo, G. Caprari, C. Rivault, M. Asadpour, F. Tâche, I. Saïd, V. Durier, S. Canonge, J. M. Amé, C. Detrain, N. Correll, A. Martinoli, F. Mondada, R. Siegwart, J. L. Deneubourg, *Science* **2007**, *318*, 1155–1158.

[2] A. Dussutour, V. Fourcassié, D. Helbing, J.-L. Deneubourg, *Nature* **2004**, *428*, 70–73.

[3] D. Helbing, W. Yu, *Proc. Natl. Acad. Sci. USA* **2009**, *106*, 3680–3685.

[4] C. K. Hemelrijk, H. Hildenbrandt, *Interface Focus* **2012**, *2*, 726–737.

[5] M. Nagy, Z. Ákos, D. Biro, T. Vicsek, *Nature* **2010**, *464*, 890–893.

[6] U. Lopez, J. Gautrais, I. D. Couzin, G. Theraulaz, *Interface Focus* **2012**, *2*, 693–707.

[7] J. Buhl, D. J. T. Sumpter, I. D. Couzin, J. J. Hale, E. Despland, E. R. Miller, S. J. Simpson, *Science* **2006**, *312*, 1402–1406.

[8] J. Werfel, K. Petersen, R. Nagpal, *Science* **2014**, *343*, 754–758.

[9] H. P. Zhang, A. Be'er, E. L. Florin, H. L. Swinney, *Proc. Natl. Acad. Sci. USA* **2010**, *107*, 13626–13630.

[10] A. Deutsch, G. Theraulaz, T. Vicsek, *Interface Focus* **2012**, *2*, 689–692.

[11] C. Chen, F. Mou, L. Xu, S. Wang, J. Guan, Z. Feng, Q. Wang, L. Kong, W. Li, J. Wang, Q. Zhang, *Adv. Mater.* **2017**, *29*, 1603374.

[12] S. Sánchez, L. Soler, J. Katuri, *Angew. Chem. Int. Ed.* **2015**, *54*, 1414–1444; *Angew. Chem.* **2015**, *127*, 1432–1464.

[13] D. Walker, P. Singh Dhruv, P. Fischer, *Adv. Mater.* **2016**, *28*, 9846–9850.

[14] M. Karimi, P. Sahandi Zangabad, S. Baghaee-Ravari, M. Ghazadeh, H. Mirshekari, M. R. Hamblin, *J. Am. Chem. Soc.* **2017**, *139*, 4584–4610.

[15] J. Li, B. Esteban-Fernández de Ávila, W. Gao, L. Zhang, J. Wang, *Sci. Robot.* **2017**, *2*, eaam6431.

[16] T. Xu, W. Gao, L. P. Xu, X. Zhang, S. Wang, *Adv. Mater.* **2017**, *29*, 1603250.

[17] J. C. Ndukaife, A. Mishra, U. Guler, A. G. A. Nnanna, S. T. Wereley, A. Boltasseva, *ACS Nano* **2014**, *8*, 9035–9043.

[18] Y. Kim, A. A. Shah, M. J. Solomon, *Nat. Commun.* **2014**, *5*, 3676.

[19] J. Li, X. Yu, M. Xu, W. Liu, E. Sandraz, H. Lan, J. Wang, S. M. Cohen, *J. Am. Chem. Soc.* **2017**, *139*, 611–614.

[20] J. Wang, Z. Xiong, J. Zheng, X. Zhan, J. Tang, *Acc. Chem. Res.* **2018**, *51*, 1957–1965.

[21] Z. Liang, D. Fan, *Sci. Adv.* **2018**, *4*, eaau0981.

[22] T. Ding, V. K. Valev, A. R. Salmon, C. J. Forman, S. K. Smoukov, O. A. Scherman, D. Frenkel, J. J. Baumberg, *Proc. Natl. Acad. Sci. USA* **2016**, *113*, 5503.

[23] S. N. Varanakkottu, M. Anyfantakis, M. Morel, S. Rudiuk, D. Baigl, *Nano Lett.* **2016**, *16*, 644–650.

[24] P. K. Kundu, D. Samanta, R. Leizrowice, B. Margulis, H. Zhao, M. Börner, T. Udayabhaskararao, D. Manna, R. Klajn, *Nat. Chem.* **2015**, *7*, 646.

[25] A. A. Solovev, E. J. Smith, C. C. Bof' Bufon, S. Sanchez, O. G. Schmidt, *Angew. Chem. Int. Ed.* **2011**, *50*, 10875–10878; *Angew. Chem.* **2011**, *123*, 11067–11070.

[26] S. Tang, F. Zhang, J. Zhao, W. Talaat, F. Soto, E. Karshalev, C. Chen, Z. Hu, X. Lu, J. Li, Z. Lin, H. Dong, X. Zhang, A. Nourhani, J. Wang, *Adv. Funct. Mater.* **2019**, *29*, 1809003.

[27] F. A. Lavergne, H. Wendehenne, T. Bäuerle, C. Bechinger, *Science* **2019**, *364*, 70–74.

[28] J. Palacci, S. Sacanna, A. P. Steinberg, D. J. Pine, P. M. Chaikin, *Science* **2013**, *339*, 936–940.

[29] D. Kagan, S. Balasubramanian, J. Wang, *Angew. Chem. Int. Ed.* **2011**, *50*, 503–506; *Angew. Chem.* **2011**, *123*, 523–526.

[30] K. Gentile, A. Somasundar, A. Bhide, A. Sen, *Chem* **2020**, *6*, 2174–2185.

[31] Z. Lin, T. Si, Z. Wu, C. Gao, X. Lin, Q. He, *Angew. Chem. Int. Ed.* **2017**, *56*, 13517–13520; *Angew. Chem.* **2017**, *129*, 13702–13705.

[32] I. Buttinoni, J. Bialké, F. Kümmel, H. Löwen, C. Bechinger, T. Speck, *Phys. Rev. Lett.* **2013**, *110*, 238301.

[33] Y. Li, H. Wang, L. Xie, Y. Liang, G. Hong, H. Dai, *J. Am. Chem. Soc.* **2011**, *133*, 7296–7299.

[34] D. Velegol, A. Garg, R. Guha, A. Kar, M. Kumar, *Soft Matter* **2016**, *12*, 4686–4703.

[35] W. Duan, R. Liu, A. Sen, *J. Am. Chem. Soc.* **2013**, *135*, 1280–1283.

[36] W. Li, X. Wu, H. Qin, Z. Zhao, H. Liu, *Adv. Funct. Mater.* **2016**, *26*, 3164–3171.

© 2021 Wiley-VCH GmbH